Title: *In vitro* 3D spheroid model preserves tumor microenvironment of hot and cold breast cancer subtypes

Running title: *In vitro* 3D spheroid model for breast cancer

Hemavathi Dhandapani, Armaan Siddiqui, Shivam Karadkar, Prakriti Tayalia*

Affiliation: Department of Biosciences and Bioengineering, Indian Institute of Technology Bombay, Powai, Mumbai, Maharashtra - 400076

*** Corresponding author.**

Corresponding author: Prof. Prakriti Tayalia, Associate Professor, Department of Biosciences and Bioengineering, Indian institute of Technology Bombay, Powai, Mumbai, Maharashtra-400076. Email: prakriti@iitb.ac.in

Abstract

Dynamic interaction of cancer, immune and stromal cells with extracellular matrix components modulates and resists the response of standard care therapies. To mimic this, we designed an *in vitro* three-dimensional (3D) spheroid model using liquid overlay method to simulate hot (MDA-MB-231) and cold (MCF-7) breast tumour microenvironment (TME). Our study shows increased mesenchymal phenotype, stemness and indoleamine-2,3-dioxygenase-1 (IDO-1) in MDA-MB-231-spheroids upon exposure to doxorubicin. Intriguingly, presence of human dermal fibroblasts enhances cancer associated fibroblast (CAF) phenotype in MDA-MB-231-spheroids through increased expression of CXCL12 and FSP-1, leading to higher infiltration of immune cells (THP-1 monocytes). However, a suppressive TME was observed in both subtypes, as seen by upregulation of M2-macrophage specific CD68 and CD206 markers. We found that addition of 1-methyl-tryptophan, a potent IDO-1 inhibitor, decreased CD206, kynurenine and IL10 expression in both hot and cold tumor subtypes, thereby, downregulating the suppressive TME. Our *in vitro* 3D spheroid model of TME can be utilized in therapeutics to validate immune-modulatory drugs for various breast cancer subtypes.

Keywords: Spheroids, MCF-7, MDA-MB-231, CXCL12, IDO-1 and IL10.

Introduction

Cancer is considered to be the leading cause of death worldwide [1] . In India, the burden of breast cancer has increased and ranks one in mortality rate [1]. Breast cancer is considered heterogeneous and is broadly classified into four subtypes based on the differences in their molecular expression. Luminal A and luminal B subtypes are positive for hormonal receptors such as estrogen and progesterone with varying levels of Ki67 expression. Her2/neu subtype is negative for hormonal receptors but shows high expression of ERBB2 receptor tyrosine kinase 2 while the triple-negative subtype lacks both hormonal and Her2/neu expression and is considered to be the most aggressive breast cancer [2]. Immunotherapy is currently recognized as the third pillar of cancer treatment after radio- and chemotherapy [3] . The upregulated expression of immune checkpoint (IC) molecules plays a major role in cancer progression and subversion of the immune system[4]. However, the success rate of various IC therapies is limited and indicates the potential of cancer models to predict the treatment outcome for various subtypes[5]. The traditional preclinical models mostly relied on 2-dimensional (2D) culture, which lack the extent of cell-to-cell contact and their crosstalk with the extracellular matrix (ECM)[6]. These models did not mimic the three-dimensional (3D) tumor microenvironment and eventually failed as they could not precisely predict the effect of drugs and immune modulators used for cancer treatments. Hence, researchers heavily depend on *in vivo* animal tumor models to understand the mechanisms of tumor initiation, invasion and drug metabolism[7] . However, the animal models lack human immune cells and are costly, laborious and time-consuming [8]. These limitations led to the development of 3D multicellular spheroids as models for mimicking the tumor microenvironment. In the TME, the formation of a hypoxic necrotic core, surrounded by a middle senescence layer and the outermost proliferating layer of cells is dependent upon the gradient of nutrients present in the surrounding region [9]. Using the spheroid model, there are studies representing MCF-7 cells with luminal subtype and MDA-MB-231 cells with triple-negative (TNBC) subtype that have shown an increase in cancer stemness upon treatment with paclitaxel and cisplatin [10]. Jingwei Li et al 2021 have observed enhanced resistance to tamoxifen treatment in 3D spheroids due to differences in chromatin architecture when compared to the 2D monolayers [11].Although these models better represent the effect of drugs likely caused by an increase in cancer stem cell phenotype, they lack the stromal component involved in tumor metastasis and immune evasion. A recent study involving co-culture of MCF-7 cells with MRC5 fibroblasts showed upregulation of alpha-SMA, indicative of their conversion to cancer-associated fibroblasts (CAF) [12]. Another study

with co-culture of MDA-MB-231 cells and CAFs revealed increased CXCL12-CXCR4 signaling which in turn induced drug resistance by activating mitogen-activated protein kinase (MAPK) and phosphoinositide 3-kinase (PI3K) pathways [13]. Macrophages are considered another major component of the TME that play a crucial role in providing treatment resistance to the tumors. Ideally, macrophages residing in the TME are referred to as tumor-associated macrophages (TAM) [14]. Many animal studies have demonstrated that TAMs are the M2 macrophages involved in enhancing angiogenesis, cancer stemness and epithelial to mesenchymal transition (EMT) [15]. This was corroborated by another study wherein targeting the CD206 expressing M2 macrophages could decrease tumor growth and prevent metastasis to lungs [16]. However, none of these studies could directly explain differences in the tumor microenvironment (TME) of luminal A and TNBC subtypes, which may provide a potential tool for targeting and validating therapeutics.

Our model comprises of 3D spheroids made via liquid overlay technique and incorporates multicellular culture to mimic TME and the cross-talk of tumor with stroma and immune cells and has been designed to compare and aid in understanding the differences between luminal A (MCF-7) and triple-negative (MDA-MB-231) subtypes of breast cancer. Our study shows a difference in the metastatic potential and an increase in cancer stemness of spheroids when compared to 2D culture. Specifically, the MDA-MB-231 spheroids show resistance to doxorubicin drug via an increase in expression of OCT3/4, NANOG and HIF1α, suggesting an increase in metastatic potential as well. Further, upon introduction of stromal fibroblasts, increased expression of cancer-associated fibroblast markers, namely CXCL12, FAP and FSP-1, leading to infiltration of THP-1 monocytes, is observed. Also, we found the expression of IDO-1 to be present only in 3D spheroids of both the subtypes and absent in the 2D culture. This led to suppression of infiltrating immune cells and an increase in conversion of macrophages into M2 phenotype as observed by CD68 and CD206 expression in the spheroids. Treatment with 1-MT, a strong IDO-1 inhibitor, led to reversal of this phenotype through reduced expression of IL-10, kynurenine and CD206. Thus, our 3D co-culture spheroid model exhibits a pro-tumor phenotype similar to an *in vivo* subtype specific TME (**Supplementary Figure 1**).

Materials and Methods

Cell Culture

MCF-7, MDA-MB-231 and HDF cells were cultured in Dulbecco's Modified Essential Media (DMEM) (GIBCO) containing 10% Fetal Bovine Serum (FBS) (GIBCO) and 1% penicillin-streptomycin-gentamicin (HiMedia) antibiotic and antimycotic. THP-1 cells were cultured in Roswell Park Memorial Institute 1640 medium (RPMI-1640) (GIBCO) supplemented with 10% FBS and 1% penicillin-streptomycin-gentamicin antibiotic and antimycotic (HiMedia).

Monoculture and coculture spheroid development

Spheroids were developed in 1.6% agarose-coated (Invitrogen) 96 well plate (Genetix Biotech Asia Pvt Ltd). MCF-7 cells (2000, 4000, 6000, 8000, 10000) and MDA-MB-231 cells (500, 1000, 1500, 2000, 3000, 4000) were suspended in 100 µl culture media per well and incubated for one hour at 37℃. Subsequently, the plates were centrifuged at 3000 rpm for 10 mins. The size and the integrity of the spheroids were monitored for 11 days through image analysis performed using IX83 Olympus microscope.

The dual culture was utilized to study the cancer-associated fibroblast markers in cocultured spheroids consisting of HDF with MCF-7/MDA-MB-231 cells at a 1:1 ratio (MCF-7 - 3000:3000, MDA-MB-231 - 1500:1500) were collected at the end of 6th day in 1 ml trizol for RNA isolation. THP-1 cells were used to co-culture with the HDF/MCF-7 and HDF/MDA-MB-231 derived breast cancer cell line. Briefly, after 24 hours of MCF-HDF (1:1) and MDA-MB-231-HDF (1:1) co-culture, the THP-1 cell line was added to both the culture at a 1:1:1 ratio (MCF-7 2000: HDF 2000: THP-1 2000, MDA-MB-231 1000: HDF 1000: THP-1 1000)[17]. To perform confocal analysis at 18 and 48 hours, spheroids were removed from the culture plate and placed in a confocal dish to check the infiltration of THP-1 cells into the spheroids. The phenotype of the infiltrating monocytes was evaluated using flow cytometry for the mentioned markers on the 6th day. The spheroids have collected and subjected to single-cell suspension using Zyme-free for 5 min (Himedia). The single cells were stained for CD45 PE, CD206 FITC, CD68 APC and CD80 PE–Cy5 (Invitrogen) immediately after staining the cells were analyzed using flow cytometry. All the antibodies are purchased from Thermo Fisher Scientific.

Live dead analysis

The viability of spheroids was assessed on the 3rd and 6th days for both MCF-7 and MDA-MB-231 cell lines. The spheroids were transferred to the new 96 well plate and incubated with

Calcein (1 µg/ml - Invitrogen) for 45 min at room temperature (RT). The Calcein stain (Invitrogen) was washed and incubated with propidium iodide (PI) (1 mg/ml - Himedia) for 5 min at RT. The PI was added immediately before imaging using confocal microscopy (LSM 780, Carl Zeiss).

Scanning electron microscopy (SEM)

Spheroids formed in agarose-coated plates were collected on the 6th day and fixed spheroids in 4% paraformaldehyde overnight at 4℃. The fixed spheroids were subsequently dehydrated with the gradient of ethanol (25%, 50%, 70%, 80% and 90%), followed by the addition of 1:2, hexamethyldisilazane (HMDS): ethanol, 2:1 HMDS: ethanol and complete HMDS. The spheroids were collected and placed onto a stub with a carbon tap, sputtered using gold target and observed under the SEM (Phenom ProX, Themo Fisher Scientific).

Quantitative real time-polymerase chain reaction (qRT-PCR)

The following genes were selected and examined by real-time PCR: PDL-1, IDO-1, TGF, Vimentin, SNAI1, SLUG, N-cadherin, E-cadherin, matrix metalloproteinase 9 (MMP9), HIF1α, αSMA, CXCL12, FAP, FSP-1, and PDGFRB. Spheroids were collected and centrifuged at 1000 rpm for 5 min. The supernatant was stored at -80℃ for ELISA analysis. The pellets were suspended in 1 ml of Trizol, the total RNA was extracted from the respective 2D and spheroid cells according to the manufacturer's instructions. After the measurement of RNA quality and quantity by nanodrop (Thermo Fisher Scientific), cDNA was synthesized using 780 ng of RNA using a cDNA synthesis kit (Thermo Fisher Scientific). Real-time polymerase chain reaction (RT-qPCR) was performed using the SYBR Premix Ex Taq II real-time PCR kit (Takara) using the QuantStudio5 (Applied Biosystem). The relative expression values of target genes were normalized with glyceraldehyde-3-phosphate dehydrogenase (GAPDH), as the internal reference gene, by using the delta-delta CT method. The list of primers and their sequence and the annealing temperature utilized was given in Supplementary Table 1.

Surface and Intracellular staining of single cell isolated from spheroids

The MDA-MB-231, and MCF-7 spheroids were collected on day 6 centrifuged and subjected to single cell dissociation either using Zyme-free (HiMedia) or trypsin (HiMedia) for 2 min at room temperature (RT). The obtained single-cell suspension cells were washed once with PBS at 1500 rpm for 5 min at RT. For testing the PDL-1 expression the cells were stained with

primary rabbit anti-human PD-L1 antibody (R&D system) for 20 min at RT in the presence of 1% bovine serum albumin (BSA)-PBS. After 20 min of incubation, the cells were stained with anti-rabbit secondary Alexa flour 488 antibody (Invitrogen) for 30 min at RT. After the staining, the cells were washed and suspended in 2% paraformaldehyde solution for further analysis.

For intracellular antibody staining, the spheroids were trypsinized into single cells followed by fixation with 4% paraformaldehyde and washed with PBS twice. Permeabilization of spheroids was done with 0.2% Triton X-100 for 15 mins and blocking was performed with 4% bovine serum albumin (BSA) PBS for 45 mins at RT. After blocking the primary antibody specific for HIF1α, OCT3/4, NANOG, and ABCB6 at 1:200 dilution (Santa Cruz biotechnology) in 4% BSA was added and incubated overnight at 4℃. The unbound primary antibody was removed by washing with 0.05% Tween 2 -PBS. Followingly, a secondary antibody conjugated with Alexa fluor 488 anti-mouse IgG secondary antibody at 1:4000 (Invitrogen) was added with 4% BSA-PBS and incubated at RT for 1 hour. The cells were acquired using a BD FACSAria flow cytometry and performed the analysis in Flowjo version 9.

Cell cycle analysis

Both the 2D and 3D cells were trypsinized and fixed with ice-cold 70% ethanol overnight at 80℃. After incubation, the cells were spun at 3000 rpm for 5 min to remove the fixative and washed cells twice with PBS. The cells were stained in 0.1% Triton-X 100 containing 20 µg/ml concentration of propidium iodide (PI) with 10 µg/ml of RNase A (Sigma-Aldrich) for 1 to 2 hours at RT for flow cytometry analysis. The cells were acquired using a BD FACSAria flow cytometry and performed the analysis in Flowjo version 9.

Determination of IC50 in 2D and 3D cultures

For 2D culture, MCF-7 and MDA-MB-231 corresponding to the luminal A and triple-negative breast cancer subtypes were seeded on a 96 well flat-bottomed cell culture plate at 10,000 cells/well in 96 culture plates for 2D. Following overnight incubation, culture media containing serially diluted anticancer drug (25000 nM to 97.6 nM) doxorubicin (DOX) was added and incubated for 72 hours at 37°C with 5% CO2. The cell viability in 2D culture was determined by measuring using the two-step MTT reagent (HiMedia). In brief, the spent culture media was removed and added 0.5 mg/ml concentration of MTT reagent in serum-free media/PBS. The cells were incubated for 4 hours at 37°C followed by the addition of DMSO to lyse the cells

and solubilize the colored formazan crystals. The colorimetric detection was done at 570 nm using the Varioskan Lux Plate Reader (Thermo Fisher Scientific). The amount of color produced is directly proportional to the number of viable cells.

For the generation of 3D culture, all the mentioned cell lines were seeded in the plate coated with 1.6% agarose (MCF-7 - 6000 cells/well, MDA-MB-231 - 3000 cells/well). After 72 hours of spheroid formation, the drug concentration was taken as mentioned above for the 2D culture. Following 72 hours of drug exposure, the multicellular spheroids were transformed into the new 96-well plate, where the MTT reagent was added and followed the same procedure to determine the cell viability.

ELISA

The secretion of suppressive cytokine (IL10), the chemokine ligand (CCL2), and IDO-1 metabolite kynurenine were quantified using the sandwich ELISA using the supernatants obtained from mono, dual and tri-culture conditions with and without the doxorubicin and 1-D/L methyl tryptophan (1-MT - Himedia) 2D and 3D culture systems. All the ELISA reagents are purchased from Krishgen Biosystems and followed the procedure as per the manufacturer protocol. The plates were scanned at 560 nm using Varioskan Lux Plate Reader.

Statistical analysis

All the statistical analysis was performed using Graphpad prism version 8.0.2. The following analysis such as unpaired parametric two-tailed T-test, IC50 determination, ordinary one-way ANOVA with Turkey's multiple comparison test and Kruskal Wallis tests was utilized to execute the statistical significance between the datasets.

Results

***In vitro* 3D spheroid model simulates an invasive breast cancer subtype**

Spheroids were developed from MDA-MB-231/MDA or MCF-7/MCF cells using liquid overlay technique with varying cell seeding densities ranging from 500-4000 cells/well for MDA and 4000-10000 cells/well MCF cells. MCF spheroids showed initial compaction until day 7 followed by an increase in size until day 11 **(Supplementary Figure 2a)**. On the other hand, MDA spheroids gradually increased in size until day 9 and eventually disintegrated by day 11 **(Supplementary Figure 2b)**. The scanning electron microscopy (SEM) images of MCF

spheroids showed enhanced extracellular matrix (ECM) deposition leading to compaction and increase in size (**Supplementary Figure 3a**) whereas MDA spheroids were smaller and had visible single cell morphology which might be leading to disintegration of spheroids by day 11 (**Supplementary Figure 3b**). The size of spheroids increased with increasing cell density in both models. Viability analysis of both tumor spheroids via Calcein/PI staining showed healthy spheroids until day 3 and necrotic core formation and cell death by day 6, as seen via uniform expression of Calcein on day 3 and an increase in PI intensity on day 6 (**Figure 1a**). HIF1α, a marker for hypoxia, while absent until day 3, showed marked presence by day 6 in the MCF spheroids, and a gradual day-wise increase in case of MDA spheroids when compared to their respective 2D cultures (**Figure 1b**).

Reports have shown that increase in hypoxia induces epithelial to mesenchymal transition (EMT) and plays a major role in imparting metastatic properties to tumours [18]. In our study also, HIF1α played a role in the expression of EMT markers. E-cadherin was significantly upregulated and N-cadherin downregulated in MCF spheroids when compared to the 2D culture exhibiting the epithelial and non-invasive phenotype of luminal cancer (**Figure 1c and 1d**). On the contrary, expression of E-cadherin was significantly downregulated and N-cadherin upregulated in MDA spheroids by day 6, indicating a mesenchymal and metastatic phenotype exhibited by our spheroid model similar to TNBC subtype. Matrix metalloproteinase 9 (MMP9), which is known to promote metastasis, was found to increase in MDA spheroids, while its expression showed a reversal in MCF spheroids by day 6 (**Figure 1e**).

Although, SNAI1 and SLUG are also markers for EMT transition, vimentin, which is an intermediate filament and involved in integrity, adhesion and migration of cancer cells, is particularly important as an indicator representing mesenchymal phenotype [19]. We found vimentin to be upregulated in MDA spheroids, indicating a potent metastatic behavior **(Supplementary Figure 4a-c)**. Further, in spheroids, all cells do not have similar access to nutrients obtained from media, which may lead to an increase in the quiescence phase (G1/G0) [20]. Our study also showed an increase in G1/G0 phase for both MCF and MDA spheroids when compared with their 2D counterparts, indicating an increase in cell quiescence and decrease in G2/M phase (**Figure 1f-i**).

Figure 1

Characterization of MCF-7 and MDA-MB-231 spheroids for cell viability, hypoxia, EMT and cell cycle. (a) Cell viability analysis of MCF-7 (top) and MDA-MB-231 (bottom) spheroids on day 3 and day 6 performed using Calcein (Green) and Propidium Iodide (Red). Scale bar = 100µm. Change in mRNA expression of (b) Hypoxia (HIF-1α) and EMT markers (c) E-cadherin, (d) N-cadherin and (e) MMP-9 in spheroids of MCF-7 (top) and MDA-MB-231 (bottom) cells when compared to their 2D culture on day 3 (D3) and day 6 (D6) analysed via qRT-PCR (n=6). (f) Cell cycle distribution analysis in 2D culture (left) and 3D spheroids (right) and (g) Quantification for MCF-7 cells via flow cytometry. (h) Cell cycle distribution analysis in 2D culture (left) and 3D spheroids (right) and (i) Quantification for MDA-MB 231 cells via flow cytometry (n=3). *p* value * ≤0.05, ** ≤ 0.01 and *** ≤0.001.

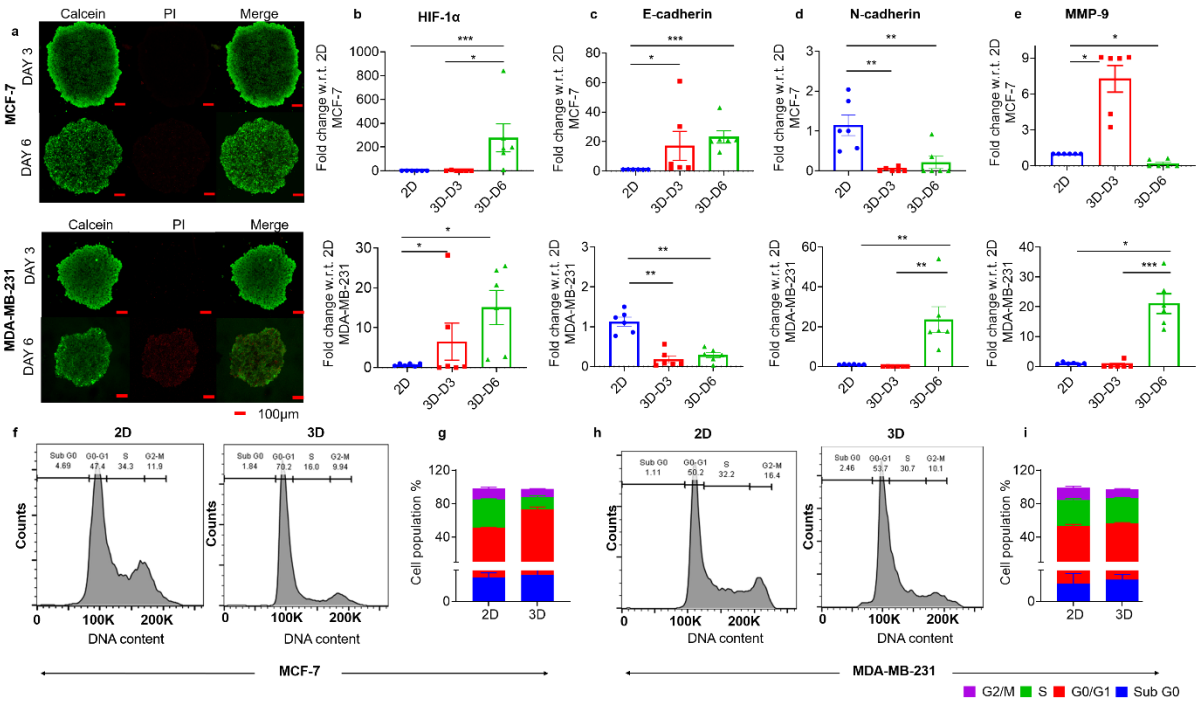

Spheroids exhibit chemoresistance via increase in cancer stemness and immune suppression

Solid tumors display resistance to therapeutics through different molecular pathways involving cancer stemness and hypoxia. To evaluate the chemotherapeutic resistance demonstrated in our 3D model, doxorubicin (DOX) was used as a chemotherapeutic drug. The concentration of drug (IC50) required to cause cell death in 3D spheroids was found to be significantly higher as compared to that in 2D culture **(Supplementary Figure 4d-e)** and led to significant

reduction in the size of both MCF and MDA spheroids **(Supplementary Figure 4f-g)**. While the levels of cancer-stemness markers (OCT3/4, NANOG, and ABCB6) seemed to increase in the 3D model when compared to 2D (for both MCF and MDA cells), they were not statistically significant, except in the case of NANOG in MDA spheroids **(Figure 2a-c)**. However, upon treatment with DOX, the levels of all the stemness markers were significantly reduced in 2D (again for both MCF and MDA) but remained unchanged for the invasive MDA spheroids, thereby indicating increased drug resistance in the 3D model as also reported *in vivo* [21]. Even the expression of HIF1α, which indicates necrosis as well as cancer stemness, showed similar behaviour between 2D vs 3D spheroid model in case of invasive MDA cells **(Figure 2d)**.

Figure 2

Increased chemoresistance in 3D spheroids as seen by cancer stem cell markers. Change in protein expression of cancer stem cell markers (a) OCT3/4 (b) NANOG (c) ABCB6 and hypoxia marker (d) HIF-1α observed via flow cytometry as seen by histograms and bar graphs comparing 2D culture and 3D spheroids in the presence and absence of doxorubicin (Dox) for MCF-7 (left) and MDA-MB-231 (right) cells (n=3). ns - not significant, *p* value * ≤0.05, ** ≤ 0.01 and *** ≤0.001.

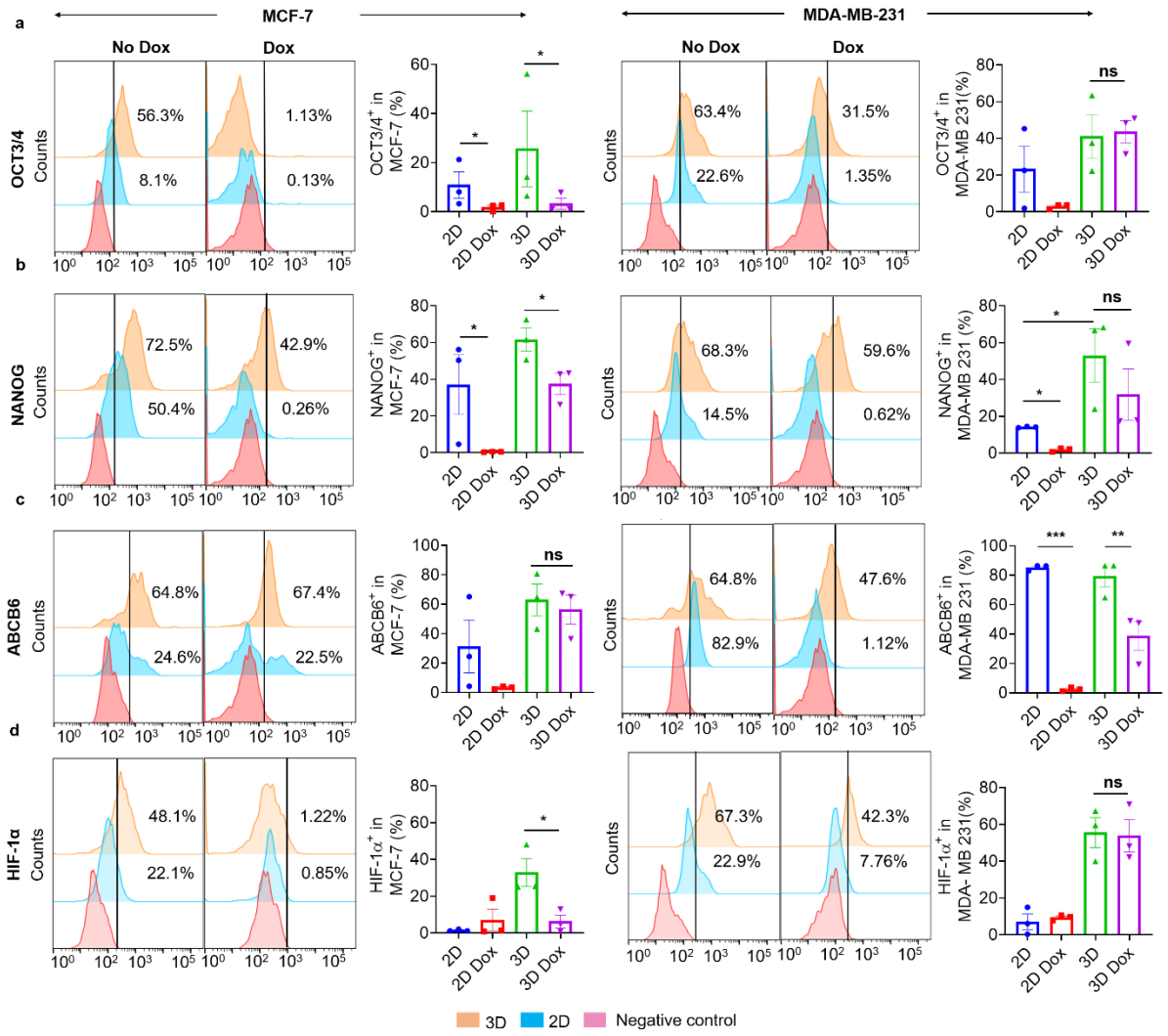

Cancer cells express certain factors, which are known to maintain pluripotency and suppress immune response, thereby enhancing tumor survival. In our study, we explored the expression of immunomodulators like PDL-1, IDO-1 and TGF-β. Again, we saw a differential response to the drug when comparing the invasive MDA subtype to the luminal and less invasive MCF subtype in our 3D model **(Figure 3a-c)**. While the expression of PDL-1 was minimal in MCF 2D culture and increased slightly in 3D spheroids, it was found to significantly decrease in MDA spheroids compared to 2D **(Figure 3a)**. We also confirmed this through protein expression of PDL-1 analyzed via flow cytometry **(Figure 3b)**. Rom-Jurek EM et al [22] have reported that hot and cold tumors regulate PDL-1 expression differently, which is consistent with our observation of differently regulated PDL-1 expression in MDA and MCF spheroids. To further corroborate the response of our 3D model to drugs, we found that upon treatment with DOX, the expression of PDL-1 did not show any change for any of the subtypes at the transcript level **(Figure 3a)**, reflecting better resemblance of our 3D invasive model to

physiological conditions. We also examined the presence of indoleamine-2,3-dioxygenase-1 (IDO-1) known to be responsible for immunosuppression in cancer [23]. While we observed a prominent increase in the expression of IDO-1 in our 3D spheroid model when compared to the respective 2D cultures, its expression increased further upon treatment with DOX, (especially for invasive subtype), indicating immunosuppression **(Figure 3c)**. In fact, for MDA spheroids, even the expression of TGF-β (another immunosuppressive factor) was enhanced upon drug treatment, which was not observed in either of the 2D cultures and did not change for MCF spheroids upon drug treatment **(Figure 3d)**. This model presents data to support the reason for failure of chemotherapy observed in patients, likely resulting from immunosuppression, suggested by the expression of IDO-1, PDL-1 and TGF-beta in response to drug **(Figure 3e)**.

Figure 3

Upregulation of suppressive immunomodulators in 3D spheroids. (a) Change in mRNA expression of PDL-1 comparing 2D culture and 3D spheroids in the presence and absence of doxorubicin (Dox) for MCF-7 (left) and MDA-MB-231 (right) cells (n=6). (b) Change in protein expression of PDL-1 observed via flow cytometry as seen by histograms and bar graphs comparing 2D culture and 3D spheroids for MCF-7 (left) and MDA-MB-231 (right) cells (n=3). Change in mRNA expression of (c) IDO-1 and (d) TGF-□ comparing 2D culture and 3D spheroids in the presence and absence of doxorubicin (Dox) for MCF-7 (left) and MDA-MB-231 (right) cells (n=6). (e) Schematic showing the regulation of various immunomodulators comparing 2D culture and 3D spheroids of MCF-7 and MDA-MB-231 cells upon treatment with doxorubicin. *p* value * ≤0.05, ** ≤ 0.01 and *** ≤0.001

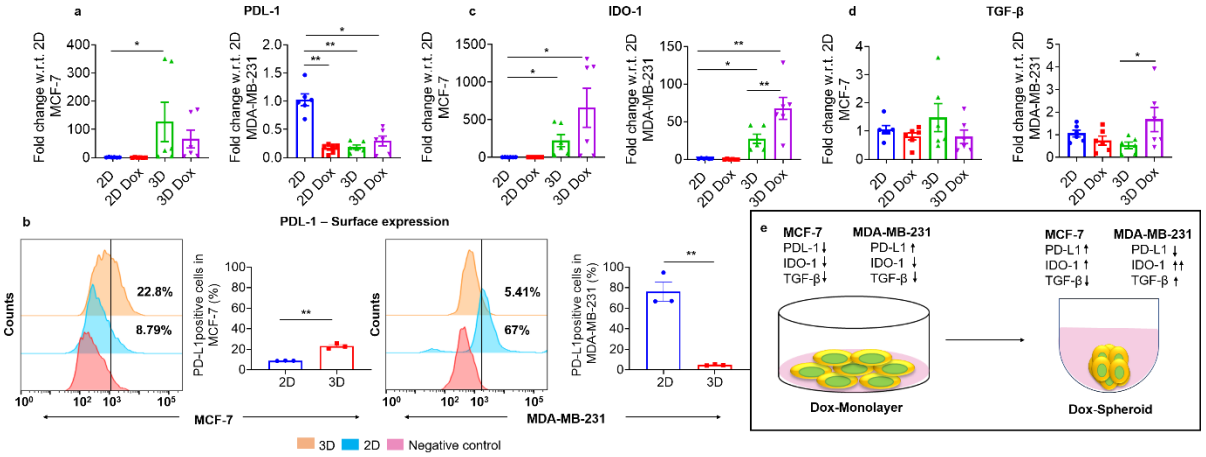

Stromal component tips the TME towards immunosuppressive phenotype while increasing immune cell infiltration.

Cancer-associated fibroblasts (CAF) are a prominent component of tumor microenvironment (TME) influencing the aggressiveness of breast cancer via altered secretion of extracellular matrix and suppression of the function of immune cells. To study the conversion of human dermal fibroblast (HDF) cells into CAF phenotype upon coculture in tumor spheroids, we analyzed the differential expression of CAF markers in both subtypes, as shown schematically in (**Figure 4a**). The distribution of HDF cells was confined to the centre in MCF spheroids whereas it was spread uniformly in MDA spheroids **(Figure 4b)**. Further, there was an upregulation of CAF markers confirming the activation of fibroblasts in cocultured spheroids **(Figure 4c-e)**. While the expression of CXCL12 increased with introduction of HDF cells in MCF spheroids, this upregulation was much more pronounced as seen by higher statistical significance in case of MDA spheroids (**Figure 4c**). Although there wasn't much change in the expression of fibroblast specific protein-1 (FSP-1) (**Figure 4d**) and fibroblast activation protein (FAP) (**Figure 4e**) in MCF cocultured spheroids, a significant increase was observed for the corresponding MDA spheroids. An increase in the expression of these CAF markers upon introduction of HDF cells in MDA spheroids suggests they acquire an aggressive phenotype with increasing stromal milieu, as also found in TNBC subtype [24,25]. The αSMA and platelet-derived growth factor receptor B (PDGFRB) were upregulated for both spheroids, indicating some heterogeneity in the two subtypes. (**Supplementary Figure 5a-b**).

Figure 4

Differential expression of CAF markers in 3D spheroids when cocultured with stromal cells. (a) Schematic showing experimental procedure for coculture of stromal cells with cancer cells leading to activation of CAF markers. (b) Spatial distribution of fibroblast cells in co-cultured MCF-7 (left) and MDA-MB-231 (right) spheroids as seen by confocal images showing MCF-7/MDA-MB-231 (red) and HDF (green) cells. Change in mRNA expression of CAF markers (c) CXCL12, (d) FSP-1 and (e) FAP in 3D spheroids for MCF-7 (top) and MDA-MB-231 (bottom) cells when cocultured with HDF cells (n=6). *p* value * $\leq$0.05, ** $\leq$ 0.01 and *** $\leq$0.001

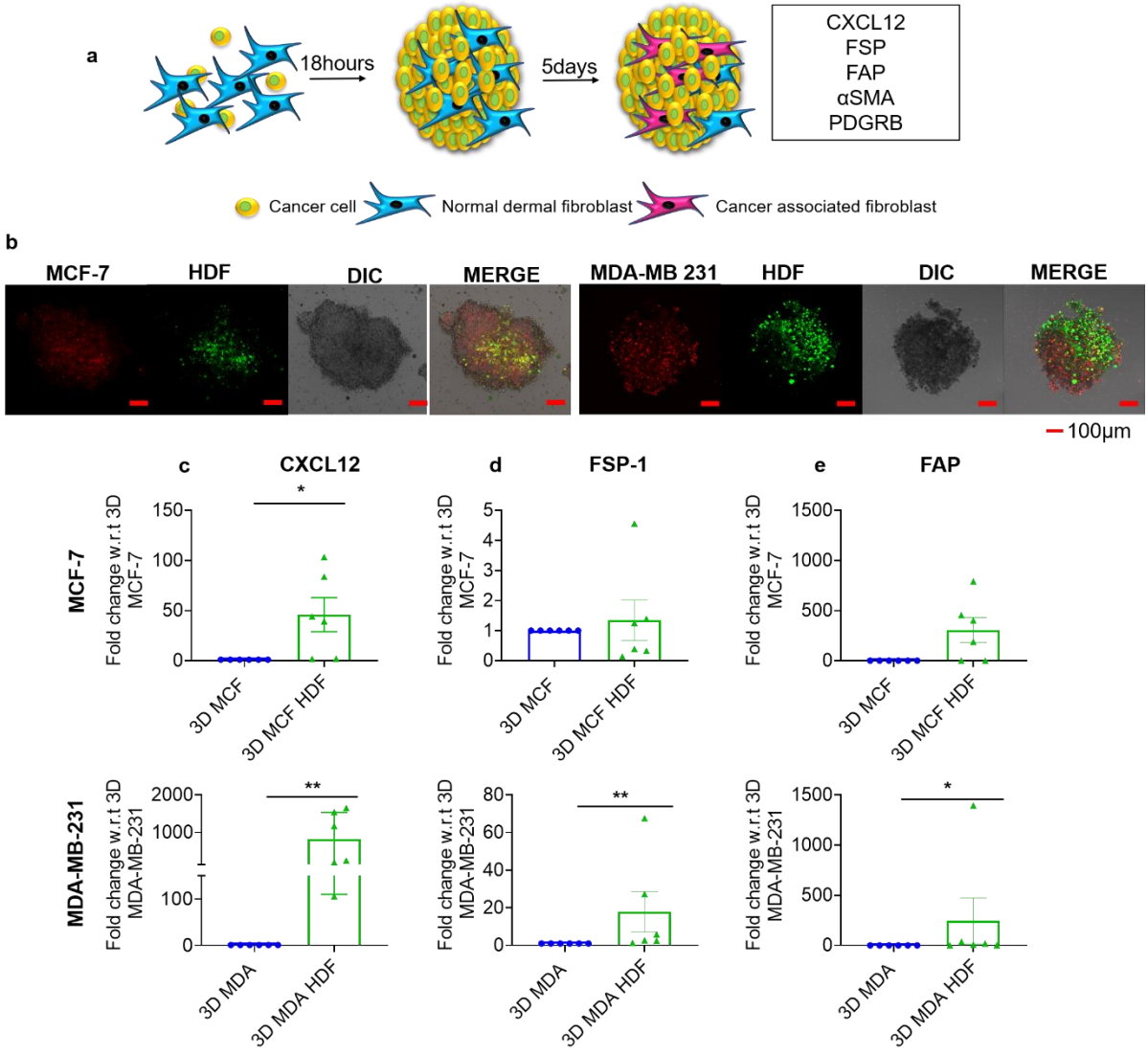

These cocultured spheroids were then incubated with THP-1 monocytes to study immune cell infiltration (**Figure 5a**). Although not much difference was seen between the two spheroids at 18 hours, a significant infiltration was observed in MDA cocultured spheroids at 48 hours as seen in the confocal fluorescence images indicating an early infiltration in hot tumors (**Figure 5b-c**). The monocytes were allowed to infiltrate for additional 72 hours and then assessed for their conversion into macrophages by analyzing the expression of CD68, CD206 and CD80 markers (**Figure 5d-e, Supplementary Figure 6a**). CD68 (**Figure 5d**) and CD206 (**Figure 5e**) were upregulated in both spheroid systems indicating the conversion of monocytes to M2-like macrophages. Further, CD80, which is characteristic of M1-like phenotype, was found to decrease in MCF spheroids, although no change was observed for their MDA counterparts (**Supplementary Figure 6b**). Upon addition of 0.5 mM of 1-MT (an IDO-1 inhibitor), both CD68 and CD206 were significantly downregulated in MCF spheroids, while the response in

MDA spheroids suggested a suppressive TME in the TNBC subtype (**Figure 5d-e**). Dose dependent response of the two subtypes to 1-MT has been shown in **Supplementary Figure 6b-c**. These results suggest that an increased expression of CAF markers in MDA spheroids facilitate an augmented recruitment of monocytes. The overall immunosuppressive phenotype exhibited by the TNBC subtype, as demonstrated in this study, shows that our model can be used as a platform to screen the immune modulatory drugs and their effect on immune cells.

Figure 5

Characterizing the differentiation of infiltrated monocytes in 3D spheroids. (a) Schematic showing experimental procedure for coculture of stromal and immune cells with cancer cells leading to differentiation of monocytes to macrophages. Confocal images represented by DIC (left), red fluorescence due CMTPX labeled monocytes (middle) and merged images (right) showing infiltrating monocytes in (b) MCF-7 and (c) MDA-MB-231 spheroids. Characterization of monocyte differentiation seen by CD45+, CD68+ and CD206+ markers upon infiltration in (d,e) MCF-7 and (f,g) MDA-MB-231 spheroids in the presence and absence of 1-MT (n=3). *p* value * $\leq$0.05, ** $\leq$ 0.01 and *** $\leq$0.001

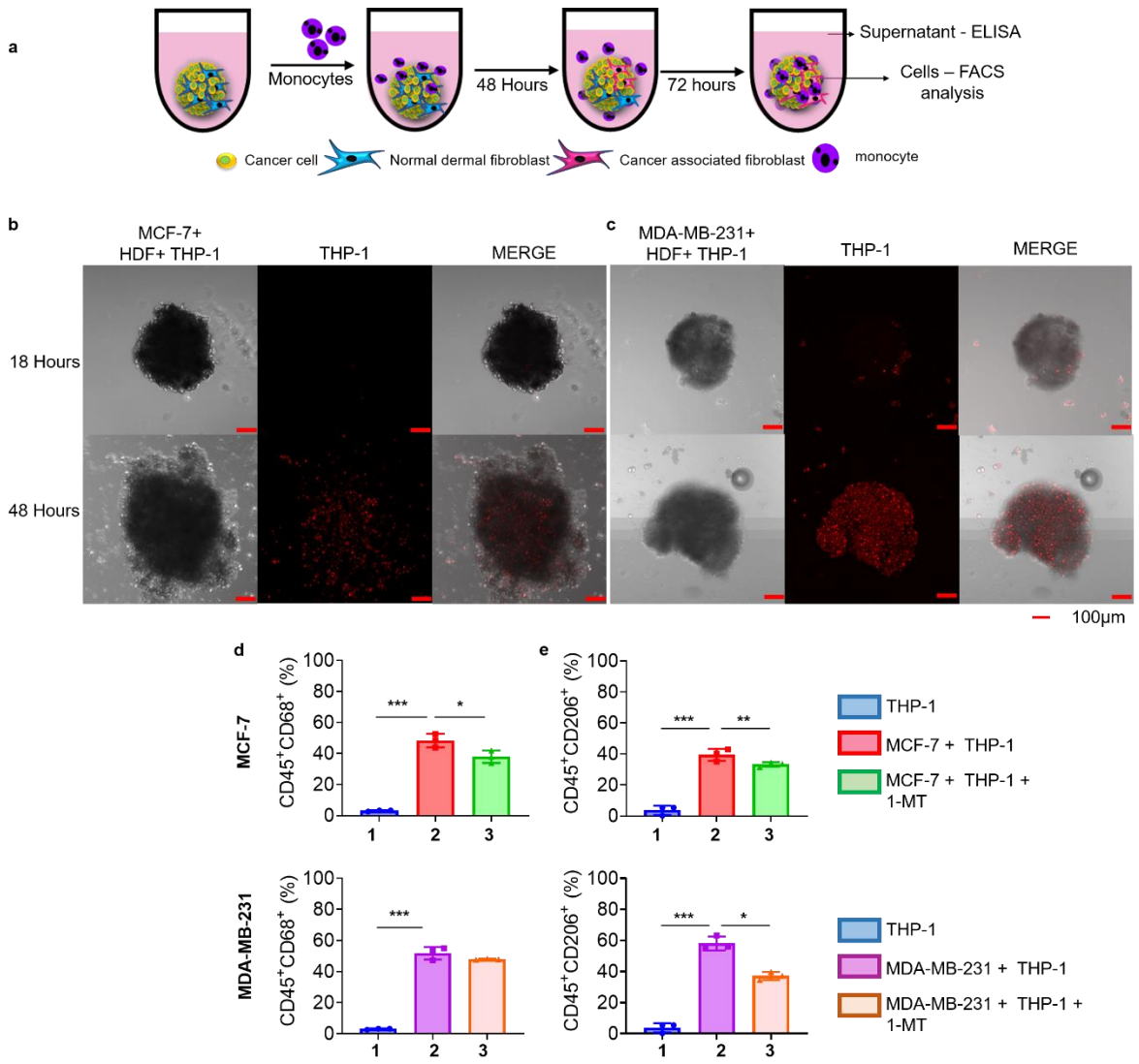

Multicellular spheroids better mimic the breast cancer TME

TME of solid tumor comprises various immune cells belonging to the innate and adaptive immune system, such as T cells, dendritic cells and macrophages. Amongst them, macrophages are the most abundant infiltrating immune cells termed as tumour associated macrophages (TAM) and are involved in the subversion of other immune cells via their plasticity [14]. As mentioned in the previous section, there was a prominent difference in the infiltration of monocytes between the two breast cancer subtypes as shown by our 3D model. Hence, we assessed the chemokines and cytokines that could be responsible for recruitment and polarization of immune cells in the TME. We found that CCL2, which is involved in the infiltration of monocytes, was secreted by MDA cells both in 2D and 3D condition, while it was completely absent in the case of MCF cells (**Supplementary Figure 7a**). Upon doxorubicin treatment, however, we found substantial increase in CCL2 for both MCF and

MDA 2D cultures, while no response was observed for their corresponding 3D spheroid systems. This could be due to increased DNA damage through direct exposure of DOX in 2D cultures, which is limited in 3D spheroids [26]. Further, when HDF cells were introduced in the co-culture systems, the secretion of CCL2 was found to increase across all conditions, signifying the role of stromal content in both luminal and TNBC subtypes. While the secretion of IL10, a suppressive cytokine, was absent in MCF cells across all culture conditions, it was found to be significantly higher in MDA cells, especially in the 3D spheroid model, which suggests its suppressive phenotype (**Supplementary Figure 7b**). Further, upon coculture with HDF cells, the IL10 secretion was still absent in MCF 2D condition, while it was significantly upregulated in the MCF spheroid model, suggesting that they acquire a suppressive phenotype in the 3D model (**Figure 6a and Supplementary Figure 7b**). On the other hand, the MDA cells represented their suppressive phenotype both in 2D as well as in 3D coculture condition. Further, with addition of 1-MT, an IDO-1 inhibitor, in the triculture condition, we found a significant decrease in IL10 secretion for the MCF system. However, for the MDA triculture, the decrease was insignificant, indicating its resistive phenotype.

Further, as we know, indoleamine-2,3-dioxygenase-1 (IDO-1), is responsible for immunosuppression in cancer and is also a rate-limiting metabolic enzyme involved in catabolism of tryptophan to kynurenine [23]. Hence, we checked for the presence of kynurenine in our system to correlate it with the presence of IDO-1. While we did not see any difference in the MCF and MDA monoculture conditions, we found that the introduction of HDF cells led to an increase in kynurenine (**Supplementary Figure 7c**). Further, to study the effect of drug responsiveness of our 3D model, we used THP-1 cells to represent the immune cell population in the TME and introduced them into the coculture of cancer cells and fibroblasts. The introduction of THP-1 itself did not change the kynurenine levels for the cocultures, however, the exposure to 1-MT led to significant reduction for both luminal and TNBC subtypes (**Figure 6b and Supplementary Figure 7c**). Furthermore, our data revealed a strong correlation between CD206 expression and IL10 secretion although such a correlation was missing with the presence of kynurenine, suggesting IL10 might have more of a direct role in the conversion of macrophages to M2-like phenotype (**Figure 6c**).

Figure 6

Effect of 1-MT on expression of suppressive markers for MCF-7 and MDA-MB-231 3D coculture spheroids. Change in expression of (a) IL10 (n=4). and (b) Kynurenine (n=4). in 3D spheroids of MCF-7 (left) and MDA-MB-231 (right) cells when cocultured with stromal and immune cells in the presence and absence of 1-MT. (c) Correlation of IL10 (left) and

Kynurenine (right) expression with presence of CD45+CD206+ cells. ns – not significant, *p* value * ≤0.05, ** ≤ 0.01 and *** ≤0.001

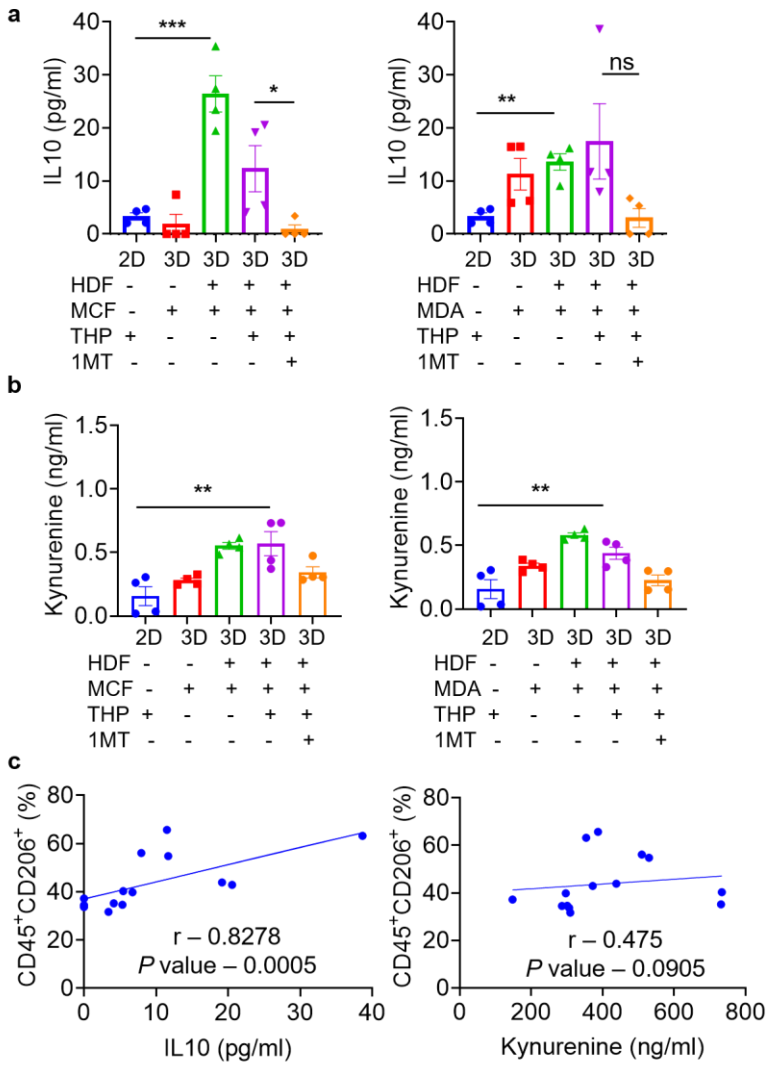

Discussion

In the current study, we developed an *in vitro* 3D model of tumor microenvironment (TME) to represent hot (triple-negative) and cold (luminal) breast tumor subtypes. We used MDA and MCF cells respectively, which formed spheroids within 3 days and maintained integrity until about 9 days (**Supplementary Figure 2a-b**). We found that HIF-1α, which is known to play a role in EMT via angiogenesis, metabolic reprogramming and survival of tumor cells [27], showed early presence in MDA and late appearance in MCF, as demonstrated by our 3D model, supporting their respective phenotypes (**Figure 1b**). Earlier studies [28] have shown the

implication of increasing HIF-1a on EMT markers suggesting the role of higher E-cadherin in formation of MCF spheroids via tight cell-cell adhesions in the current study (**Figure 1c**). Likewise, our studies demonstrated a significant increase in the expression of N-cadherin and MMP-9 in MDA spheroids (**Figure 1d-e**), thereby, confirming the metastatic potential of these cells in 3D [29]. On par with other studies [30], we found the cells in our 3D model to have more quiescent G1/G0 phase cells in the cell cycle (**Figure 1f-i**) as well as higher dose response to chemotherapeutic drugs (**Supplemetary Figure 4d-e**) compared to their 2D counterparts, similar to what is expected in an *in vivo* tumor scenario [31].

Even the cancer stemness markers, such as OCT3/4 and NANOG, which are known to support the long-term self-renewal capacity of tumor cells [32], were found to upregulate in MDA spheroids, which demonstrated chemoresistance by maintaining their levels of expression upon DOX treatment (**Figure 2a-b**). Similar behavior was observed for TGFβ expression (**Figure 3d**), which is also known to induce EMT [33]. PDL-1, which contributes to immunosuppression, is associated with an increase in triple-negative when compared to luminal breast cancer subtype [34]. However, Rom-Jurek et al 2018 have shown higher expression of PDL-1 in 2D monolayer culture when compared to the *in vivo* animal retrieved tumors of MDA cells [22]. In our study as well, we found the expression of PDL-1 in MDA to be downregulated as the culture conditions were changed from 2D culture to 3D spheroid model (**Figure 3a-b**). Further, this expression was maintained upon doxorubicin drug treatment suggesting acquisition of chemoresistive phenotype in 3D model.

It is known that indoleamine-2,3-dioxygenase-1 (IDO-1) is also involved in immunosuppression and is responsible for conversion of tryptophan to kynurenine, thereby increasing the regulatory phenotype of TME infiltrating immune cells [35]. Clinical studies have also shown a strong correlation of IDO-1 activity with dense stromal lymphocytic infiltration in TNBC patients, suggesting basal phenotype [36]. In our study as well, both MCF and MDA spheroids showed higher IDO-1 expression as compared to their monolayer cultures, however, upon doxorubicin treatment, this expression was found to be upregulated only for the corresponding TNBC subtype represented by the MDA spheroids.

CAFs play a vital role in reprogramming breast cancer cells via ECM remodeling and cancer-associated inflammation leading to therapeutic resistance. Recent studies have also indicated

transition from a cancer cell-centric to a stroma-centric therapeutic strategy, which may hold promise due to stable gene expression of the stromal cells [37,38]. In our study, we looked at the various CAF markers, which could also be used as potential therapeutic targets. Specifically, we found a higher fold expression of CXCL12 for MDA spheroids when compared to their MCF counterparts (**Figure 4c**), which is inline with the malignant progression of TNBC observed in animal studies [39]. Other CAF related markers such as fibroblast activation protein (FAP) and fibroblast specific protein-1 (FSP-1) were also found to be upregulated in the MDA coculture model while no difference was observed in the corresponding MCF system (**Figure 4d-e**). This is in agreement with a recent study which showed that an increase in FAP production leads to degradation of extracellular matrix (ECM) through increased accumulation of MMP-9, which is known to enhance the metastatic behavior of breast cancer [40]. In contrast, the expression of αSMA was found to increase in our MCF co-culture condition (**Supplementary Figure 5a**), which is also in agreement with an earlier clinical study showing an increase in alpha SMA and promoting the growth of luminal breast cancer subtype [41]. Additionally, increased expression of CXCL12 enhances the infiltration and differentiation of monocytes into more suppressive macrophages and accelerates metastatic potential in the TME of breast cancer [42]. It is also known that tumor-associated macrophages (TAMs) play a vital role in the suppression of immune system and activation of malignant cells thereby accelerating metastasis [43]. In our studies as well, we observed an increased infiltration of monocytes in the metastatic model (MDA triculture) (**Figure 5b**), which is on par with earlier studies showing heightened infiltration of macrophages in breast cancer-derived tumor [44]. Even increased expression of FSP-1 is known to promote differentiation of monocytes to M2-type macrophages [45]. This is also aligned with our MDA model showing an increased expression of FSP-1 leading to larger infiltration of CD206 expressing macrophages in comparison to the MCF model (**Figure 5c-e**). Moreover, secretion of IL10 and CCL2 was predominant in metastatic breast cancer preventing apoptosis of cancer cells upon chemotherapy [46]. We have also observed secretion of IL10 and CCL2 in MDA monoculture spheroids, which was completely absent in the MCF system (**Supplementary Figure 7a-b**), suggesting a suppressive phenotype in the basal-like TNBC subtype [47]. Intriguingly, our studies show secretion of IL10 and CCL2 in the MCF coculture spheroids (**Supplementary Figure 7a-b**), suggesting that infiltration of activated fibroblasts can reshape the microenvironment of luminal type breast cancer to more aggressive phenotype. IL10 is also known to influence expression of M2-like macrophages through IDO-1 [48]. This relates with our *in vitro* model, wherein overexpression

of IDO-1 leads to an increase in IL10 and kynurenine metabolite, as also observed in other studies [49]. 1-MT, which is currently used in clinics to treat various solid tumors, has shown improved anti-tumor efficacy when used as a combination therapy [50]. It overcomes immune perturbation and stimulates M1 phenotype in the infiltrating monocytes [51]. Our data corroborates with these studies wherein the addition of 1MT decreases tryptophan conversion to kynurenine and reduces the expression of IL10, potentially leading to anti-tumor response. This sets up our model as a platform for studying the TME of hot and cold breast cancer subtypes and for screening immunomodulators and chemotherapeutics.

In conclusion, our *in vitro* model was shown to mimic the tumour microenvironment of basal-like model through increase in N-cadherin and MMP9 production, and that of the luminal model through upregulation of E-cadherin. Our 3D model showed resistance to doxorubicin through increase in cancer cell stemness and upregulation of IDO-1 expression when compared to 2D monolayer. Increase in differentiation of infiltrating THP-1 to M2-like macrophages synchronized with upregulation of CAF markers such as CXCL12, FAP and FSP-1 in basal-like subtype. Finally, addition of an IDO-1 inhibitor restrained the immunosuppressive microenvironment by reducing CD206 and IL10 expression. Thus, our *in vitro* model very closely recreates an *in vivo* TME and can potentially be used as a platform to test the effect of therapeutics in cancer. We can further develop this model for performing mechanistic studies and understanding the role of immunomodulators in various cancer subtypes (**Supplementary Figure 8**).

Declarations

Ethics approval and consent to participate

Not applicable.

Consent for publication

Not applicable.

Availability of data and material

The authors can share the data upon request.

Competing Interest

The authors declare that there are no competing interests regarding the publication of this paper.

Funding

We thank the Science and Engineering Research Board (SERB) for providing the funds for conducting research (Grant No: CRG/2021/003710).

Author contribution

P.T., H.D. and A.S. conceptualized and designed the study. H.D. and A.S. performed all the experiments, analysed the data, and wrote first draft of the manuscript. S.K. helped with some preliminary experiments. P.T. supervised the study, provided funding, and critically reviewed the manuscript.

Acknowledgement

We acknowledge Ms. Saranya Ajesh for imaging spheroids using SEM, CRNTS and Department of Biosciences and Bioengineering at IIT Bombay for usage of flow cytometry and confocal microscopy instrumentation facility.

Reference

[1] H. Sung, J. Ferlay, R. L. Siegel, M. Laversanne, I. Soerjomataram, A. Jemal, F. Bray, *CA Cancer J Clin* **2021**, *71*, 209.

[2] U. Testa, G. Castelli, E. Pelosi, *Med Sci (Basel)* **2020**, *8*, 18.

[3] G. Deslypere, D. Gullentops, E. Wauters, J. Vansteenkiste, *Ther Adv Med Oncol* **2018**, *10*, DOI 10.1177/1758835918772810.

[4] V. C. Brom, C. Burger, D. C. Wirtz, F. A. Schildberg, *Front Immunol* **2022**, *13*, DOI 10.3389/FIMMU.2022.837645.

[5] X. He, C. Xu, *Cell Res* **2020**, *30*, 660.

[6] S. Martinez-Pacheco, L. O'driscoll, *Cancers (Basel)* **2021**, *13*, DOI 10.3390/CANCERS13236033/S1.

[7] H. Gabbert, *Cancer Metastasis Rev* **1985**, *4*, 293.

[8] G. Bahcecioglu, G. Basara, B. W. Ellis, X. Ren, P. Zorlutuna, *Acta Biomater* **2020**, *106*, 1.

[9] P. S. Sankar, M. F. C. Mat, K. Muniandy, B. L. S. Xiang, P. S. Ling, S. L. L. Hoe, A. S. B. Khoo, N. Mohana-Kumaran, *Oncol Lett* **2017**, *13*, 2034.

[10] D. S. Reynolds, K. M. Tevis, W. A. Blessing, Y. L. Colson, M. H. Zaman, M. W. Grinstaff, *Sci Rep* **2017**, *7*, DOI 10.1038/S41598-017-10863-4.

[11] J. Li, K. Fang, L. Choppavarapu, K. Yang, Y. Yang, J. Wang, R. Cao, I. Jatoi, V. X. Jin, *Clin Epigenetics* **2021**, *13*, DOI 10.1186/S13148-021-01167-6.

[12] I. Yakavets, A. Francois, A. Benoit, J. L. Merlin, L. Bezdetnaya, G. Vogin, *Sci Rep* **2020**, *10*, DOI 10.1038/S41598-020-78087-7.

[13] S. L. Ham, P. S. Thakuri, M. Plaster, J. Li, K. E. Luker, G. D. Luker, H. Tavana, *Oncotarget* **2017**, *9*, 249.

[14] I. Vitale, G. Manic, L. M. Coussens, G. Kroemer, L. Galluzzi, *Cell Metab* **2019**, *30*, 36.

[15] D. Cruceriu, O. Baldasici, O. Balacescu, I. Berindan-Neagoe, *Cell Oncol (Dordr)* **2020**, *43*, DOI 10.1007/S13402-019-00489-1.

[16] C. Zhang, L. Gao, Y. Cai, H. Liu, D. Gao, J. Lai, B. Jia, F. Wang, Z. Liu, *Biomaterials* **2016**, *84*, 1.

[17] S. P. Rebelo, C. Pinto, T. R. Martins, N. Harrer, M. F. Estrada, P. Loza-Alvarez, J. Cabeçadas, P. M. Alves, E. J. Gualda, W. Sommergruber, et al., *Biomaterials* **2018**, *163*, 185.

[18] J. P. Joseph, M. K. Harishankar, A. A. Pillai, A. Devi, *Oral Oncol* **2018**, *80*, 23.

[19] K. Strouhalova, M. Přechová, A. Gandalovičová, J. Brábek, M. Gregor, D. Rosel, *Cancers (Basel)* **2020**, *12*, DOI 10.3390/CANCERS12010184.

[20] C. H. Huang, K. F. Lei, N. M. Tsang, *Biotechnol Prog* **2019**, *35*, e2787.

[21] D. Biswas, L. Slade, L. Duffley, N. Mueller, K. T. Dao, A. Mercer, S. Pakkiriswami, Y. el Hiani, P. C. Kienesberger, T. Pulinilkunnil, *Cell Death Discovery 2021 7:1* **2021**, *7*, 1.

[22] E. M. Rom-Jurek, N. Kirchhammer, P. Ugocsai, O. Ortmann, A. K. Wege, G. Brockhoff, *International Journal of Molecular Sciences 2018, Vol. 19, Page 563* **2018**, *19*, 563.

[23] L. Zhai, E. Ladomersky, A. Lenzen, B. Nguyen, R. Patel, K. L. Lauing, M. Wu, D. A. Wainwright, *Cell Mol Immunol* **2018**, *15*, 447.

[24] K. Takai, A. Le, V. M. Weaver, Z. Werb, *Oncotarget* **2016**, *7*, 82889.

[25] J. Zhou, X. H. Wang, Y. X. Zhao, C. Chen, X. Y. Xu, Q. Sun, H. Y. Wu, M. Chen, J. F. Sang, L. Su, et al., *J Cancer* **2018**, *9*, 4635.

[26] V. Levina, Y. Su, B. Nolen, X. Liu, Y. Gordin, M. Lee, A. Lokshin, E. Gorelik, *Int J Cancer* **2008**, *123*, 2031.

[27] R. Y. Ebright, M. A. Zachariah, D. S. Micalizzi, B. S. Wittner, K. L. Niederhoffer, L. T. Nieman, B. Chirn, D. F. Wiley, B. Wesley, B. Shaw, et al., *Nat Commun* **2020**, *11*, DOI 10.1038/S41467-020-20144-W.

[28] A. Ivascu, M. Kubbies, *Int J Oncol* **2007**, *31*, 1403.

[29] R. B. Hazan, G. R. Phillips, R. F. Qiao, L. Norton, S. A. Aaronson, *J Cell Biol* **2000**, *148*, 779.

[30] J. Laurent, C. Frongia, M. Cazales, O. Mondesert, B. Ducommun, V. Lobjois, *BMC Cancer* **2013**, *13*, DOI 10.1186/1471-2407-13-73.

[31] Y. Imamura, T. Mukohara, Y. Shimono, Y. Funakoshi, N. Chayahara, M. Toyoda, N. Kiyota, S. Takao, S. Kono, T. Nakatsura, et al., *Oncol Rep* **2015**, *33*, 1837.

[32] D. Wang, P. Lu, H. Zhang, M. Luo, X. Zhang, X. Wei, J. Gao, Z. Zhao, C. Liu, *Oncotarget* **2014**, *5*, 10803.

[33] G. Wu, Y. Li, *BMC Pharmacol Toxicol* **2022**, *23*, 1.

[34] H. R. Ali, S. E. Glont, F. M. Blows, E. Provenzano, S. J. Dawson, B. Liu, L. Hiller, J. Dunn, C. J. Poole, S. Bowden, et al., *Annals of Oncology* **2015**, *26*, 1488.

[35] X. Zhao, Y. Jiang, M. Xu, J. Hu, N. Feng, H. Deng, C. Lu, T. Huang, *Toxicol Appl Pharmacol* **2022**, *440*, DOI 10.1016/J.TAAP.2022.115921.

[36] S. Kim, S. Park, M. S. Cho, W. Lim, B. I. Moon, S. H. Sung, *J Cancer* **2017**, *8*, 124.

[37] J. Tchou, J. Conejo-Garcia, *Adv Pharmacol* **2012**, *65*, 45.

[38] H. Luo, G. Tu, Z. Liu, M. Liu, *Cancer Lett* **2015**, *361*, 155.

[39] M. Yang, C. Zeng, P. Li, L. Qian, B. Ding, L. Huang, G. Li, H. Jiang, N. Gong, W. Wu, *Onco Targets Ther* **2019**, *12*, 3849.

[40] Y. Huang, A. E. Simms, A. Mazur, S. Wang, N. R. León, B. Jones, N. Aziz, T. Kelly, *Clin Exp Metastasis* **2011**, *28*, 567.

[41] A. Muchlińska, A. Nagel, M. Popęda, J. Szade, M. Niemira, J. Zieliński, J. Skokowski, N. Bednarz-Knoll, A. J. Żaczek, *Cell Mol Biol Lett* **2022**, *27*, 1.

[42] P. J. Boimel, T. Smirnova, Z. N. Zhou, J. Wyckoff, H. Park, S. J. Coniglio, B. Z. Qian, E. R. Stanley, D. Cox, J. W. Pollard, et al., *Breast Cancer Res* **2012**, *14*, DOI 10.1186/BCR3108.

[43] S. Chen, C. Shao, M. Xu, J. Ji, Y. Xie, Y. Lei, X. Wang, *Int J Clin Exp Pathol* **2015**, *8*, 9052.

[44] C. Ni, L. Yang, Q. Xu, H. Yuan, W. Wang, W. Xia, D. Gong, W. Zhang, K. Yu, *J Cancer* **2019**, *10*, 4463.

[45] L. Prasmickaite, E. M. Tenstad, S. Pettersen, S. Jabeen, E. v. Egeland, S. Nord, A. Pandya, M. H. Haugen, V. N. Kristensen, A. L. Børresen-Dale, et al., *Mol Oncol* **2018**, *12*, 1540.

[46] T. Kitamura, B. Z. Qian, D. Soong, L. Cassetta, R. Noy, G. Sugano, Y. Kato, J. Li, J. W. Pollard, *J Exp Med* **2015**, *212*, 1043.

[47] D. A. Stewart, Y. Yang, L. Makowski, M. A. Troester, *Mol Cancer Res* **2012**, *10*, 727.

[48] X. F. Wang, H. S. Wang, H. Wang, F. Zhang, K. F. Wang, Q. Guo, G. Zhang, S. H. Cai, J. Du, *Cell Immunol* **2014**, *289*, 42.

[49] G. C. Prendergast, C. Smith, S. Thomas, L. Mandik-Nayak, L. Laury-Kleintop, R. Metz, A. J. Muller, *Cancer Immunol Immunother* **2014**, *63*, 721.

[50] R. Hong, Y. Zhou, X. Tian, L. Wang, X. Wu, *Int Immunopharmacol* **2018**, *54*, 118.

[51] F. Guo, M. Hu, D. Huang, Y. Zhao, B. Heng, G. Guillemin, C. K. Lim, W. J. Hawthorne, S. Yi, *Xenotransplantation* **2017**, *24*, DOI 10.1111/XEN.12326.